PCCP

Accepted Manuscript

ROYAL SOCIETY OF CHEMISTRY

www.rsc.org/pccp

Interstellar H Adsorption and H_2 Formation on the Crystalline (010) Forsterite Surface. A B3LYP-D2* Periodic Study

Javier Navarro-Ruiz[a], Mariona Sodupe[a], Piero Ugliengo[b] and Albert Rimola[a]*

[a] *Departament de Química, Universitat Autònoma de Barcelona, 08193 Bellaterra, (Spain)*

[b] *Dipartimento di Chimica and NIS Centre, Università degli Studi di Torino, Via P. Giuria 7, 10125 Torino (Italy)*

Abstract

The physisorption/chemisorption of atomic hydrogen on a slab model of the Mg_2SiO_4 forsterite (010) surface mimicking the interstellar dust particle surface has been modeled using a quantum mechanical approach based on periodic B3LYP-D2* density functional calculations (DFT) combined with flexible polarized Gaussian type basis sets, which allows a balanced description of the hydrogen/surface interactions for both minima and activated complexes. Physisorption of hydrogen is barrierless, very weak and occurs either close to surface oxygen atoms or on Mg surface ions. The contribution of dispersion interactions accounts for almost half of the adsorption energy. Both the hydrogen adsorption energy and barrier to hydrogen jump between equivalent surface sites are overestimated compared to experimental results meant to simulate the interstellar conditions in the laboratory. Hydrogen atom exclusively chemisorbs at the oxygen site of the forsterite (010) surface, forming a SiOH surface group and its spin density being entirely transferred to the neighboring Mg ion. Barrier for chemisorption

allows a rapid attachment of H at the surface at 100 K, but prevents the same process to occur at 10 K. From this H-chemisorbed state, second hydrogen chemisorption mainly occurs on the neighboring Mg ion, thus forming a Mg-H surface group, giving rise to a surface species stabilized by favorable electrostatic interactions between the OH^+/H^-Mg pair. The formation of molecular hydrogen at the (010) forsterite surface adopting a Langmuir-Hinshelwood mechanism takes place either starting from two physisorbed H atoms with an almost negligible kinetic barrier through a spin-spin coupling driven reaction or from two chemisorbed H atoms with a barrier surmountable already at T higher than 10 K. We also suggest that a nanosized model of the interstellar dust built from a replica of the forsterite unit cell is able to adsorb half the energy released by the H_2 formation by increasing its temperature by about 50 K which could then radiates in about 0.02 s.

Introduction

H_2 is one of the most relevant molecules in the Universe. It is the most abundant molecule in the interstellar medium (ISM), an effective coolant for gases and of clouds during gravitational collapse and plays a crucial role in the formation of other interstellar molecular species.[1, 2] Because of that, formation of H_2 in the ISM is a process of fundamental importance in astrophysics.

Gas-phase H_2 formation cannot justify the observed H_2 large abundances. Radiative association of two H atoms is a very low efficient process. Indeed, association through the first electronic excited state cannot radiate through the ground electronic state due to spin forbidden selection rule, while the transitions from excited to ground-state H_2 ro-vibrational states are only possible through a very inefficient electric

quadrupole coupling due to the H_2 symmetry. Non-radiative association is also highly inefficient, as the formed H_2 cannot transfer the chemical bond energy (about 104 kcal mol^{-1}) in absence of a third body with consequent immediate re-dissociation. Three-body reactions are indeed extremely rare, due to the very low densities of the ISM (about 100 H atoms cm^{-3}). Thus, it has been long recognized[3] that one of the most effective H_2 formation channel involves dust grains, which play the role of a large third body dispersing a fraction of the H_2 formation energy through the phonon grain manifold. The assessment of this hypothesis has been checked by a wealth of experimental studies carried out in Earth laboratories on the formation of H_2 at surfaces of model dust analogs.[1, 2]

In the ISM, dust grains are formed in the extended atmosphere of relatively cold stars or in the expelled shells after Supernovae explosions. In diffuse clouds, where typical gas densities are about 10^2 cm^{-3} and gas temperatures about 80–100 K, UV photons are able to penetrate the cloud and, accordingly, dust grains are in a bare state, most of the gas being either in an atomic form or as simple diatomic species, with a great preponderance of H_2. More complex molecules, if formed, are easily photo-destroyed. Dust consists of Mg/Fe-silicates and carbonaceous materials, with the former belonging to olivines and pyroxenes families, with general formula $Mg_{2x}Fe_{(2x-2)}SiO_4$ and $Mg_xFe_{(x-1)}SiO_3$ (x=0–1), respectively. Cosmic silicates are mainly present as amorphous materials, but crystalline silicates have also been detected in several circumstellar environments.[4-6]

H_2 formation on dust grains can take place via three possible mechanisms: i) Langmuir-Hinshelwood,[7, 8] which involves accommodation, diffusion and reaction of H atoms on the surface; ii) Eley-Rideal "prompt atom",[9, 10] in which an incoming gas-phase H atom directly reacts with a pre-adsorbed surface H atom; and iii) Harris-

Kasemo "hot-atom",[11] in which an H atom with high translation energy reaches the surface, diffuses loosing part of its translational energy and reacts with a pre-adsorbed H atom. Irrespective on the mechanism, understanding the H adsorption, which involves different physical/chemical interactions (*i.e.* physisorption/chemisorption), is a key prerequisite to understand the subsequent recombination.

Several theoretical works focusing on the H_2 formation on carbonaceous surface models (*i.e.* coronene clusters and C(0001) surfaces) have been published,[12-15] generally predicting a high reaction probability and significant ro-vibration populations in nascent molecules, in agreement with the experimental findings.[16] Usually, effects due to the presence of porous and point defects were not accounted for.

Few theoretically studies dealt with the H adsorption and the H_2 formation on silicate surfaces, in which the latter is simulated either by nano-clusters or by periodic approaches using crystalline surfaces. The works by Bromley and coworkers[17, 18] belong to the first category, in which $(MgO)_6((SiO)_2)_3$ and $Mg_4Si_4O_{12}$ silicate nano-clusters were adopted as dust models and both H adsorption and recombination were studied with DFT methods and Gaussian type basis sets. Garcia-Gil et al.[19] exhaustively explored different H adsorption sites on the Mg_2SiO_4 (010) surface by means of periodic calculations at the PBE level and Gaussian type basis set ranging between double and triple-zeta polarized quality as encoded in the SIESTA program, showing that the most favorable physisorption site is on the Mg atom and the chemisorption one on the neighboring O atom. Downing et al.[20] studied the H adsorption on the (010) crystal termination of both forsterite and fayalite using a PBE functional and plane wave basis set as encoded in the VASP program, finding chemisorption on both Mg and O sites. Goumans et al.[21] adopted an embedded (QM/MM) approach in which a cluster model of the (010) crystalline forsterite surface containing 55 atoms is treated quantum

mechanically with the MPWB1K functional and Gaussian basis set of polarized double zeta quality and is embedded in a large array of point charges providing the long range Coulomb contribution. They found the important result that the simultaneous H adsorption on the Mg and O surface sites yields the formation of a hydride (H^-) and a proton (H^+), respectively, the recombination of which was found to be energetically very favorable. This point was essential to establish a route to the formation of molecular H_2 through chemisorbed H atoms, which is operative at relatively high temperature (diffuse clouds, T=100 K) in which the H physisorbed state would be unstable.

The available theoretical works only addressed the reactants paths starting from the H atoms accommodated on the most stable sites, while the reaction channels that connect one adsorption state into another one have not been fully characterized. This is an important issue because at the very low temperatures at which these processes occur the inter-conversion between two adsorption sites could be kinetically hampered. The available results dealing with the H_2 formation on silicate grains missed in general the role of dispersion interactions, with the exceptions of Ref.[17, 21], as they are based on the meta-GGA MPWB1K functional, which was showed to be the best among various functionals to take weak interactions into account.[22] The role of dispersive forces cannot be ignored as, for instance, it has been recently shown that they are essential to accurately model the CO adsorption on the crystalline (001) face of MgO resulting in an interaction energy value of only 4.5 kcal mol^{-1}.[23-25] It is then expected that dispersion may play a similar role in describing the H and H_2 physisorption on the forsterite (010) surface which has electric property comparable to that of MgO. Following the good results found in the above papers, we present here a coherent approach based on the adoption of *a posteriori* Grimme's-based dispersion corrected B3LYP-D2*

Hamiltonian[26, 27] in a flexible Gaussian basis set to characterize the H adsorption and H_2 formation on the (010) crystalline face of forsterite (Mg_2SiO_4) represented by a slab model of finite thickness. Different adsorption sites as well as the corresponding inter-conversion activated complexes and the corresponding energy paths have been characterized. The sensitivity of the adsorption energies on the quality of basis set and of the adopted Hamiltonian has been carefully checked. For all the possible singly H-adsorbed complexes, the adsorption of a second H atom has been considered and from these doubly-adsorbed complexes, H_2 formation has been simulated adopting a Langmuir-Hinshelwood mechanism. This work is the first of a series in which the Hamiltonian, the surface structural model and the computer program (CRYSTAL09) are used to coherently characterize the bare forsterite surfaces[28] and their interaction with molecules of interstellar interest.

Methods

Surface Model. In this work a periodic surface model of the non-polar (010) forsterite surface has been adopted. This surface was derived from cutting out the forsterite crystal bulk structure (*Pbnm* space symmetry) perpendicular to the [010] direction, resulting with the slab model shown in Figure 1. A larger unit cell compared to the primitive cell derived from the direct cut of the bulk system has been adopted (*i.e.* the bulk *c* lattice parameter is doubled in the slab). The resulting surface model contains 56 atoms per unit cell and has a thickness in the [010] cut direction, after geometry relaxation, close to the original *b* value (10.254 Å)[28] of the bulk unit cell from which the slab has been derived. A very recent work of us[28] presents an exhaustive discussion on the reconstruction effects, structural parameters and physico-chemical properties of this

surface. Here, it is worth to highlight that this surface model is terminated by under-coordinated Mg^{2+} cations (*i.e.*, they are coordinated by three O atoms compared to the octahedral coordination for a bulk Mg^{2+} ion) resulting in electrostatic potential map showing prominent positive and negative valued regions associated to the outermost Mg and O surface ions, respectively.

Computational Details. All calculations were carried out by using the periodic ab initio code CRYSTAL09.[29, 30] All the SCF calculations and geometry optimizations were performed in *P1* group symmetry using the B3LYP-D2* density functional method, which includes an empirical *a posteriori* correction term proposed by Grimme[26] to account for dispersion forces (missed in the pure B3LYP[31] method), but whose initial parameterization (D2) was modified for extended systems (D2*),[27] to provide accurate results for the calculations of cohesive energies of molecular crystals and of adsorption processes within a periodic treatment.[23-25] Moreover, for the adsorption of one H atom, single point energy calculations using the PBE,[32] BLYP,[33, 34] and BHLYP[35] density functional methods at the B3LYP-D2* optimized geometries have also been performed in order to check the influence of the method on the computed adsorption energies. Transition state (TS) search has been performed using the distinguished reaction coordinate (DRC) technique as implemented in CRYSTAL09, which has been proven to be robust and efficient enough for the proton jump of nonhydrated and hydrated acidic zeolites.[36] The activated complex structures corresponding to the TS have been checked by ensuring that only one imaginary frequency resulted by the Hessian matrix diagonalization. All calculations involving one H atom have been run as open-shell systems based on the unrestricted formalism. Electron spin densities on the atoms have been obtained by using the Mulliken population analysis.

For the atoms belonging to the forsterite surface, two different Gaussian basis sets have been adopted starting from previous works focused on the forsterite[28]: i) a B1 basis set described by the following all-electron contractions: (8s)-(831sp)-(1d) for Si; (6s)-(31sp)-(1d) for O; (6s)-(631sp)-(1d) for the top-layer Mg atoms (standard 6-31G(d,p) Pople basis set); and (8s)-(61sp)-(1d) for the remaining Mg atoms; and ii) a B2 basis set described by the larger all-electron contractions: (8s)-(6311sp)-(1d) for Si; (8s)-(411sp)-(1d) for O; (631111s)-(42111p)-(1d) for the top-layer Mg atoms (standard 6-311G(d,p) Pople basis set); and (8s)-(511sp)-(1d) for the remaining Mg atoms.[28] For all calculations, a TZP basis set from the Ahlrichs and coworkers[37] has been used for the H atoms. Optimizations using both the B1 and B2 basis set have been carried. Moreover, single point energy calculations at B2 onto the optimized B1 geometries have also been performed (hereafter referred as B2//B1) to save computer time.

The shrinking factor of the reciprocal space net, defining the mesh of *k* points in the irreducible Brillouin zone, was set to 5 and 20 for B1 and B2 calculations, respectively, which requires the diagonalization of the Hamiltonian matrix in 3 and 6 *k* points, respectively. The accuracy of both Coulomb and exchange series was set to values of overlap integrals of 10^{-6} and 10^{-16} for both B1 and B2. A pruned (75, 974) grid (CRYSTAL09 keyword XLGRID) has been used for the Gauss–Legendre and Lebedev quadrature schemes in the evaluation of functionals. The condition to achieve SCF convergence between two subsequent cycles was set to 10^{-7} Hartree. Relaxations of the internal atomic coordinates have been carried out by means of analytical energy gradients[38] keeping the lattice parameters fixed at the bulk values. The geometry optimization was performed by means of a quasi-Newton algorithm in which the quadratic step (BFGS Hessian updating scheme) is combined with a linear one as proposed by Schlegel.[39]

The adsorption energies (ΔE) *per* mole of a H atom and *per* unit cell were computed as:

$$\Delta E = E(\mathrm{SH//SH}) - E(\mathrm{S//S}) - E_{\mathrm{m}}(\mathrm{H})$$

where E(SH//SH) is the energy of the relaxed unitary cell containing the forsterite surface S in interaction with the H atom, E(S//S) is the energy of the relaxed unitary cell of the free forsterite surface, and E_m(H) is the energy of the free H atom (the symbol following the double slash identifies the geometry at which the energy was computed). Because Gaussian basis functions were used, the above ΔE definition suffers from the basis set superposition error (BSSE). The above equation can be easily recast to include the BSSE correction, using the same counterpoise method adopted for intermolecular complexes.[40] The definition of the BSSE-corrected adsorption energy ΔE^{C} is:

$$\Delta E^{\mathrm{C}} = \Delta E^{*\mathrm{C}} + \delta E_{\mathrm{S}}$$

$$\Delta E^{*\mathrm{C}} = E(\mathrm{SH//SH}) - E(\mathrm{S[H]//SH}) - E(\mathrm{[S]H//SH})$$

in which δE_{S} is the deformation energy of the forsterite surface due to the adsorption of the H atom (note that δE_{H} is null), E(S[H]//SH) is the energy of the forsterite surface plus the ghost functions of H, and E([S]H//SH) is the energy of the infinite replica of H with the ghost functions of the forsterite surface. For the sake of brevity, we refer to previous works for a complete discussion concerning the calculation of the ΔE^{C} and the associated BSSE values.[40] Kinetic constants k^{TST} have been computed by standard transition state theory using partition functions and the activation free energy. H tunneling has also been considered in a rather crude way by means of the Wigner correction $\kappa = 1 + \frac{1}{24}\left(\frac{h\nu^{\neq}i}{k_B T}\right)^2$ in which $\nu^{\neq}$ is the imaginary frequency associated to the

activated complex.[41] The final kinetic constant is then simply $k = \kappa \times k^{TST}$. To facilitate the comparison with other computed or experimental results of astrochemical interest adsorption/desorption energies and reaction barriers data reported on Tables 1, 3 and 4 are shown using kcal mol^{-1}, meV and K units, respectively.

CRYSTAL09 computes the zero-point energy (ZPE) corrections and the thermodynamic quantities by the standard statistical thermodynamics formulas based on partition functions derived from the harmonic oscillator approximations which are used to correct the adsorption energy values by temperature effects. Vibrational frequencies of the considered systems were computed at the Γ point (point k=0 in the first Brillouin zone, called central zone) within the harmonic approximation by obtaining the eigenvalues from diagonalization of the mass-weighted Hessian matrix. This dynamical matrix was obtained by numerical differentiation (central-difference formula) of the analytical first-energy derivatives, calculated at the geometries obtained by varying, in turn, each of the 3N equilibrium nuclear coordinates by a small amount u = 0.003 Å. For more detailed discussion on the computational conditions and other numerical aspects related to calculation of the vibrational frequencies at the Γ point see Ref.[42] For the considered systems in this work, building up the full mass-weighted Hessian matrix would have been very expensive because N atoms in the unit cell implies performing 3N+1 energy *plus* gradient calculations in the central-difference formula, so that only a portion of the dynamical matrix was computed by considering the displacements of a subset of atoms; *i.e.*, the H atoms and the first and second-layered atoms of the surface (see Figure 1 for a detailed view of the included atoms).

Results and Discussion

This section is organized as follows. First, results devoted to the H adsorption on the (010) forsterite (hereafter referred as Fo) surface will be presented. In this part, the influence of both the DFT methods and the basis sets on the calculated adsorption energies is discussed. Then, the energy profiles connecting the different adsorption sites will also be discussed. Results focused on the adsorption of a second H atom will be shown and finally, the energy profiles for the H_2 formation from the doubly adsorbed pre-reactant states adopting a Langmuir-Hinshelwood mechanism will be presented. This mechanism is alternative to the Eley-Rideal[9,10] one in which the outer H atom hits the pre-adsorbed H atom at the grain surface which has been studied in details for the H_2 formation on graphite like grains.[12,13,16] In a very low H flux regime as in diffuse clouds it seems reasonable to assume the Langmuir-Hinshelwood as the dominant process, particularly when one of the adsorbed H is long lived due to the formation of a chemical bond with the surface.[15]

Adsorption of one H atom. Figure 2 shows the B3LYP-D2* optimized complexes for the adsorption of one H atom on the Fo surface. Table 1 and Table 2 report the adsorption energies calculated at the different B1 and B2 basis set and the different DFT methods, respectively.

Three different H/Fo complexes have been found, which, according to the calculated adsorption energies, can be categorized as physisorption (P1 and P2) and chemisorption (C1), respectively. In P1, the H atom is nearly on the center of a triangle defined by three oxygen surface atoms; in P2, the H atom is interacting with one coordinatively unsaturated Mg atom and in C1, the H atom is chemically bonded with an O atom, hence forming a surface silanol (SiOH) group. For P1 and P2, the Mulliken

spin density is almost entirely localized on the H atom, whereas for C1 is on the unsaturated neighbor Mg atom, the H atom having a character of H^+ (see Table 2 for details). The trend of the calculated B3LYP-D2* adsorption energies is, from more to less favorable: C1 > P2 > P1 (see Table 1). The contribution of the dispersive forces (term ΔE_{D2*} of Table 1) is larger in P1 (by about the 55% of the total adsorption energy) than in P2 and C1 (13% and 2%, respectively). The higher dispersion contribution in P1 compared to P2 is basically due to a higher number of intermolecular contacts between the adsorbed H and the forsterite surface atoms. The inclusion of the zero-point energy (ZPE) corrections is mandatory as it causes a lowering of the adsorption energies by about 30% – 50%.

From a methodological point of view it is worth highlighting that, for a given adsorption state, the calculated adsorption energies at B2 and B2//B1 are very similar (difference of 0.3 kcal mol^{-1}, at the most) and have similar BSSE values, whereas at B1 the BSSE is about twice as large of that at B2. This indicates that calculations at B2//B1 provide accurate results at a reasonable computational cost. Adsorption energies calculated with different DFT methods on the optimized B3LYP-D2* structures (see Table 2) vary compared to those obtained with the default B3LYP-D2* method. It results that for the B-LYP family the larger stability of P2 with respect to P1 decreases with the amount of exact exchange to the point that at BHLYP-D2* P2 is less stable than P1, *i.e.*, the P2-P1 relative energies are -2.0, -1.0 and +0.4 kcal mol^{-1}, at BLYP-D2*, B3LYP-D2* and BHLYP-D2*, respectively. The Mulliken spin densities are less sensitive to the level of calculation than the ΔE values.

Figure 3a shows the B3LYP-D2* energy profiles (including ZPE corrections) for the conversion of the P1 and P2 physisorbed configurations into the C1 chemisorbed

state following the P1 → P2 → C1 path. Table 3 shows the corresponding energy barriers and kinetic constants. The conversion from P1 to P2 involves the diffusion of the H atom on the Mg atom, whereas from P2 to C1 involves the formation of a surface O-H bond at the expenses of the partial breaking of the outermost Mg-O bond. As expected, the energy barrier of the first step is computed to be lower than the second one (4.0 and 6.3 kcal mol^{-1}, respectively, at B2//B1) since in the latter Mg-O bond breakings occur. However, the calculated transition structures are higher in energy than the Fo + H asymptote, thus indicating that the jump from one site to another one may occur through H desorption/adsorption steps rather than via surface diffusion. To deepen into this point, localization of transition structures that connect the Fo + H asymptote with the adsorbed states have been attempted. For P1 and P2, no transition structures have been found; *i.e.*, the DRC calculations show a continuous increase of energy up to a plateau with the increased Fo-H distance. In contrast, a transition structure for C1 has indeed been found with an energy barrier of 6.0 kcal mol^{-1} at the B2//B1 basis set (see Figure 3b) very close to the value obtained for passing from P2 to C1 (see Figure 3a). The barrier computed for passing from the physisorption P2 structure to the chemisorbed state C1 is 6.4 kcal mol^{-1} (see Table 3), much higher than the value of 1.7 kcal mol^{-1} computed by Kerkeni and Bromley on the forsterite nanoclusters[17] and of that of 2.4 kcal mol^{-1} reported by Goumans et al.[21] for the embedded cluster method. While these differences may well be due to the different computational approaches, we admit that other paths for passing from P2 to C1 have not been searched due to difficulties in locating the transition structure with the implemented algorithm. For instance, the path through surface oxygen ions rather than the Mg ion (see TS_{P1-P2} of Figure 3a) may provide a smaller barrier.

Any attempt to locate other adsorption sites by starting the optimization process with the H atom closer to a different oxygen atom or on top of Mg ions simply gave P1, P2 or C1 as final products. This is somehow at variance with the work by Sidis et al.[19] in which H was predicted to remain attached to a second less exposed oxygen atom as well as with the results by Downing et al.,[20] in which H was predicted to chemisorb also at the surface Mg ion. Nevertheless, for both cases the adsorption was much less favorable than for the cases also (and only) found in the present work.

Present results can be compared with the experimental measurements reported in the classical work by Vidali and Pirronello.[43] They extracted energy values from thermal desorption experiments (TPD) giving both the physisorbed H desorption energy and the barrier height for H jumping from one site to the next neighbor. As the formal treatment of TPD data corresponds to an Arrhenius equation their desorption energy data E_a should be transformed in enthalpy values before being compared with the computed ones.[23] The experimental and computed enthalpy of desorption ΔH_d are:

$$\Delta H_d = E_a - RT \qquad \text{(from experiment)}$$

$$\Delta H_d = -\Delta E^C - \Delta E(\text{ZPE}) - \Delta E(\text{T}) + \text{RT} = -\Delta U^C - \Delta E(\text{T}) + \text{RT} \qquad \text{(from theory)}$$

in which E_a is the experimental desorption energy resulting from the Arrhenius equation, $-\Delta E^C$ is the purely BSSE corrected electronic desorption energy, $-\Delta U^C$ is the desorption energy inclusive of zero point energy correction and $-\Delta E(\text{T})$ is the thermal correction to bring ΔU^C to the actual T (from 10 to 100 K). It can be shown that the $-\Delta E(\text{T})$ is less than 0.05 kcal mol^{-1} (2 meV, 20 K) while RT is 0.02 kcal mol^{-1} (1 meV, 10 K) at 10 K and ten times higher at T = 100 K. Using data from Table 1 we arrive at our best estimate of ΔH_d = 1.8 kcal mol^{-1} (900 K) at the experimental temperature of 10

K. The datum obtained from the experimental TPD measurements[43] is 318 K, three times smaller than our best estimate. Modeling studies described in the introduction section report data which are also higher than the experimental datum. As none of these data have been corrected for zero point energy and thermal effects we use our electronic ΔE^{C} = 2.7 kcal mol^{-1} value for comparison, which corresponds to the value of ΔH_{d} = 1.8 kcal mol^{-1} discussed above. Goumans et al.[21] computed 2.5 kcal mol^{-1}, Sidis et al.[19] a value of 3.2 kcal mol^{-1}, Kerkeni and Bromley[17] a range of values between 1.4- 5.8 kcal mol^{-1} as a function of the adsorption cluster site. Analysis of the contribution to the physisorption energy reveals that dispersion contribution is in the 0.5 – 1.6 kcal mol^{-1} range and cannot be ignored. The sensitivity of the physisorption on the adopted functional is addressed in Table 2, in which the P2 desorption energy (not accounting for BSSE) moves from 1.9 (BHLYP-D2*) up to 5.0 (PBE-D2*) kcal mol^{-1}. To reconcile experimental data with the computed one Goumans et al.[21] invoked the possible role of surface hydroxylation in the experiment which heals the active sites of forsterite. While that can be the case, our data show that different functionals may play a significative role in changing the physisorption value, which imposes some caution when using DFT for computing very weak interactions in open-shell systems. The computed value of the kinetic barrier for H jump between physisorbed sites resulted in 4.1 kcal mol^{-1} (Table 3), much higher than the experimental datum reported by Katz et al.[43] of only 0.57 kcal mol^{-1}. Goumans et al.[21] computed a value of 1.6 kcal mol^{-1} while Kerkeni and Bromley[17] a range between 0.14 - 4.8 kcal mol^{-1} as a function of the considered path on the heterogeneous cluster surface.

Adsorption of a second H atom. To simulate the formation of the H_2 molecule on the forsterite surface through a Langmuir-Hinshelwood mechanism, the adsorption of a second H atom onto the P1, P2 and C1 adducts has firstly been studied. Figure 4 shows

the B3LYP-D2* optimized adducts and Table 4 the calculated adsorption energies for the second H atom.

Since the adopted unit cell includes two equivalent but symmetry independent "Mg-O_3" moieties, a total of 9 initial guess adducts were possible: i) three with the H atoms adopting the same adsorption state at the different "Mg-O_3" moieties (*i.e.*, P1-P1, P2-P2 and C1-C1); ii) three derived from the combination of the P1, P2 and C1 adsorption states at the different "Mg-O_3" moieties (*i.e.*, C1-P1a, C1-P2a and P2-P1a); and iii) three more derived from the combination of P1, P2 and C1 at the same "Mg-O_3" moiety (*i.e.*, C1-P1b, C1-P2b and P2-P1b). All these initial guess structures have been calculated as closed-shell (singlet electronic state) systems. Geometry optimization of all these starting structures collapsed into 6 different complexes, which are shown in Figure 4. The initial P2-P1a and P2-P1b structures converged into the same adduct (structure P2-P1 of Figure 4) and the C1-P1a and C1-P1b complexes evolve toward the spontaneous formation of H_2 (the Fo-H_2 adduct, shown at the bottom of Figure 4).

The adsorption energy for this second H atom has been calculated considering the H addition reactions reported in Table 4. As one can see, the C1-P2a and C1-P2b complexes are the most stable ones (BSSE-corrected adsorption energies including ZPE-corrections, ΔU_0^C, being -61.8 and -78.7 kcal mol^{-1}, respectively). This is because these adducts contain both an hydride and a proton, which arise from the Mg-H and the Si-OH groups, respectively as first pointed out by Goumans et al.[21] These complexes are formed because in C1 the unpaired electron is almost entirely localized on the bare Mg atom (see Table 2), thereby having a large propensity to receive the second H atom to form a Mg^+-H^- hydride. The larger stability of C1-P2b with respect to C1-P2a is due to the favorable electrostatic interaction between the two H atoms, respectively with a H^-/H^+ character due to the bond with Mg/O ions (Mulliken net charges of these H atoms

are -0.35/+0.35 |*e*|, respectively). The P1-P1, P2-P1 and P2-P2 adducts give ΔU_0^C values of about -2/-3 kcal mol^{-1}, in which the spin densities are on the H atoms (with opposite signs). For the C1-C1 complex, the adsorption of the second H atom is unfavorable (ΔU_0^C = +2.5 kcal mol^{-1}) because the formation of a surface geminal Si-$(OH)_2$ group, resulted from the breaking of two Mg-O surface bonds (see structure C1-C1 of Figure 4).

H_2 formation. From the doubly H-adsorbed adducts, the recombination of the H ad-atoms to form a H_2 molecule has been studied. The B3LYP-D2* energy profiles including ZPE-corrections with respect to the 2H + Fo asymptote are shown in Figure 5 and Figure 6 and the calculated energy barriers and kinetic constants in Table 3. The reaction energy for the H_2 formation is very large and negative (about -107 kcal mol^{-1}), in agreement to the large nascent energy associated with the H_2 molecule formation. Not surprisingly, the H_2 formation when the two H atoms are physisorbed on the Fo surface (*i.e.*, P2-P1 and P2-P2) exhibit very low energy barriers (less than 1 kcal mol^{-1}, see Figure 5 and Table 3) as this process envisages a radical-radical reaction. Kinetic data of Table 3 show that association to H_2 is feasible at 10 K at higher rate for P2-P2 than for P2-P1 even without considering tunneling effects, thus suggesting that the Langmuir-Hinshelwood mechanism is feasible. It is worth mentioning that any attempt to find a reaction from the P1-P1 complex failed, since the located transition structures collapsed on the $TS_{P2\text{-}P1}$ structure (the same for the P2-P1 complex) meaning that, previous to the H_2 formation, a conversion of the P1-P1 complex into P2-P1 should take place.

The H_2 formation channels when at least one of the H atoms is chemisorbed were found to have higher energy barriers (see Figure 6 and Table 3) compared to those for the physisorbed states. However, from the C1-P2b adduct, the calculated energy

barrier is 1.7 kcal mol^{-1} (see Figure 6b and Table 3). This is because the H recombination is between the neighboring H^- and H^+ atoms belonging to the surface Mg-H and SiOH groups, respectively (*vide supra*). Despite the fact that the very same $H^-\cdots H^+$ coupling might occur for the C1-P2a, the reaction presents an energy barrier of 23 kcal mol^{-1} (see Figure 6a and Table 3). This increment is caused by the need of breaking the Mg-H bond in order to bring the two H atoms in close proximity. We have also checked whether the H of C1-P2a can first evolve towards C1-P2b (see $TS_{C1\text{-}P2ab}$ of Figure 4) but data in Table 3 show that a barrier as high as 18.3 kcal mol^{-1} is needed for this reaction, preventing any sensible occurrence of this process. Finally, the H_2 formation from the C1-C1 complex exhibits the highest energy barrier (about 35 kcal mol^{-1}, see Figure 6c and Table 3) since this recombination involves the coupling of two H^+ atoms that belong to the surface geminal $Si(OH)_2$ group.

The present results are at variance from the data computed by Goumans et al.[21] with the embedded cluster approach, as they computed a much higher barrier of 11.1 kcal mol^{-1} for the recombination of the two chemisorbed H atoms, compared to our value of 1.7 kcal mol^{-1} starting from the C1-P2b adduct. Comparison with barriers computed by Kerkeni and Bromley[17] is less straightforward as they adopted the $(MgO)_6(SiO_2)_3$ nanocluster, resulting in a rather large range of values spanning the 1.4-21.2 kcal mol^{-1} interval as a function of the hydrogen attachment sites. Nevertheless, our barrier is compatible with their smallest barrier value of 1.4 kcal mol^{-1} resulting from the formation of H_2 starting from structure 4a of Ref.[17]

The H_2 molecule is very weakly bound to the reconstructed forsterite surface resulting in an adsorption energy value corrected for the zero point energy of -2.1 kcal mol^{-1}, as shown in the last row of Table 4. Similarly to the adsorption of atomic hydrogen, dispersion contributes up to 50% to the adsorption energy. One point of

interest is to establish how the energy due to the H_2 formation (about 107 kcal mol^{-1}, see Figure 5) can be released to the internal modes of the dust particle. For H_2 to be formed, it is enough that a fraction of that energy is transferred to the dust grain while the remaining will be removed through translational, vibrational and rotational degrees of freedom of the nascent H_2. In the simplifying hypothesis that half of the formation energy is released to the dust particle, about $\Delta E \approx 50.2$ kcal mol^{-1} are then absorbed by the particle with an efficiency proportional to the particle heat capacity. We compute the molar heat capacity *per* unit cell of the free forsterite (010) slab using the harmonic frequencies for the whole bare slab model resulting in $C_V \approx 0.11$ kcal mol^{-1} K^{-1}. To represent a finite nanosized dust particle cut out from our slab model we consider a 3x3x1 unit cell size model (9 unit cells as a whole). Considering that a single unit cell parameters are a ≈ 4.8 Å, b ≈ 12 Å and c ≈ 10.3 Å (see Figure 1), the resulting volume V and external surface A of the model particle are V = 5.4×10^3 Å^3 and A = 2×10^3 Å^2, respectively. If we assume that a single H_2 molecule is formed at the surface of this grain with the same ΔE value computed for the periodic slab, the increment in absolute temperature of a dust particle is $\Delta T = \Delta E/(C_V \cdot 9) \approx 53$ K. Considering that the initial temperature of the particle is around 10 K it heats up to 63 K. Assuming the particle to behave like a perfect black body its emissive power j is given by the Stefan-Boltzman law, $j = \sigma T^4$, in which σ is the Stefan constant (5.6×10^{-8} J s^{-1} m^{-2} K^{-4}). The power (J s^{-1}) radiated by the particle is then $P = A \cdot j$ in which A is the surface of the particle (*vide supra*). From that, the time needed to radiates half of the H_2 formation energy ($\Delta E \approx$ 50.2 kcal mol^{-1}) adsorbed by the particle is then $\tau = \Delta E/P = 0.02$ s.

Conclusions and Astrochemical Implications

In this work the (010) surface of Mg_2SiO_4 forsterite has been used as a model for the core of the interstellar dust particle using a quantum mechanical approach based on periodic density functional calculations. The adsorption of atomic hydrogen and the formation of molecular hydrogen has been studied in detail using the B3LYP-D2* method combined with flexible polarized Gaussian type basis sets, which allows a balanced description of the H/surface interactions for both minima and activated complexes. The relevance of the present results to the astrochemical context are summarized in the following: i) H physisorption at the (010) surface is barrierless and exclusively occurs either on the most exposed surface oxygen (P1) or on the outermost Mg ions (P2), with a zero point energy (ZPE) corrected adsorption energy of about -2 kcal mol^{-1} (≈ -90 meV, ≈ -1000 K). Dispersion accounts for almost half of the adsorption energy; the residence time of H on the surface at 10 K is then 0.2 ps; ii) the kinetic ZPE corrected barrier for the hydrogen atom jump between the physisorption sites (*i.e.*, P1 → P2) is 4.1 kcal mol^{-1} (178 meV, 2063 K), which corresponds to a negligible value of the kinetic constant inclusive of tunnel correction at 10 K; the rate constant only becomes significant at 100 K at which H atoms have already desorbed; this implies that H diffusion is limited, at least for the simple path taken here into account, and H can only displace on the surface through adsorption/desorption steps; iii) H atom chemisorbs with a ZPE adsorption energy of -9.0 kcal mol^{-1} (-390 meV, -4529 K) and a kinetic barrier from P2 of 6.4 kcal mol^{-1} (278 meV, 3221 K) at the oxygen site of the forsterite (010) surface with spin density entirely located to the nearby Mg ion; iv) the formation of the chemisorbed state C1 through the direct interaction of the H atom is characterized by a ZPE corrected barrier of 6.0 kcal mol^{-1} (260 meV, 3019 K) high enough to hinder the process at 10 K; v) a second H atom can be chemisorbed on an already reacted Fo surface (the C1 case) to form the most stable product C1-P2b

releasing about 79 kcal mol^{-1} (3407 meV, 39607 K), which envisages a vicinal Si-OH(+)/(–)H-Mg ion pair interaction; vi) the H_2 formation at the Fo surface adopting a Langmuir-Hinshelwood mechanism starts either from two physisorbed H atoms (P2-P1 and P2-P2 adducts) with an almost negligible kinetic barrier of 0.5 kcal mol^{-1} (21 meV, 242 K) through a spin-spin coupling driven reaction, or from two chemisorbed H atoms as in the C1-P2b adduct with a barrier of 1.7 kcal mol^{-1} (74 meV, 854 K) which gives a half-life (assuming first order kinetic) of about 0.5 My at 15 K; vii) it is estimated that the released energy by the H_2 formation can be dispersed through the dust particle internal phonon modes (assuming a nanosized cuboid particle of 15×36×10 Å) and that the temperature increase 53 K due to the internal conversion of half the H_2 formation energy, which could be radiated into the space in about 0.02 s.

The present study shows that much work is still needed to fully characterize the formation of H_2 by models of forsterite dust particles. For instance, it is still unclear the reason of the large overestimation of both interaction energy and energy barrier for adsorption and diffusion for H physisorption on forsterite when compared to experiment. It may be due to the dominance of a different crystalline surface with respect to (010) one here considered or, even, as it has been suggested[21] by the healing of the most energetic sites by water contamination in the experimental chamber. On a methodological side, more rigorous approaches are needed to study this point, for instance, in the same line adopted by Martinazzo et al.[16] to study the H_2 formation on graphitic dust particle. The difficulty of being rigorous for this specific problem is the light nature of H atom, which renders even the *ab initio* molecular dynamics based on classical nuclei dynamics not accurate enough. Less doubtful, but still under scrutiny for a possible functional dependency, is the discovery that even on a forsterite crystalline surface the barrier to the H_2 recombination starting from two neighbor chemisorbed

atoms is small enough for the reaction to occur at and up 15 K temperature. Nevertheless, the present approach, rigorously grounded on a periodic representation of the forsterite crystalline surface which ensures an accurate description of the surface electrostatic field, allows a coherent comparison between the reactivity of different surfaces and to check for the role of exact exchange on the energy profiles. Results can be compared with those coming from finite cluster models of the interstellar dust as developed by Kerkeni and Bromley[17] to see to which extent the reactivity of a nanosized cluster is different from that of an extended surface which, ultimately, will improve our understanding of the structure and features of the interstellar dust.

Acknowledgements

Financial support from MICINN (projects CTQ2011-24847/BQU and CTQ2013-40347-ERC) and DIUE (project 2009SGR-638) is gratefully acknowledged. J.N.-R. is indebted to SUR of ECO of Generalitat de Catalunya for a predoctoral grant. A.R. is indebted to MICINN of the Spanish Government for a Juan de la Cierva contract. M.S. gratefully acknowledges support through 2011 ICREA Award. P.U. acknowledges Progetti di Ricerca di Ateneo-Compagnia di San Paolo-2011-Linea 1A, progetto ORTO11RRT5 for funding. A. R. kindly acknowledges BSC-MN for the generous allowance of computing time through the "QCM-2013-2-0006: Formation of Molecular Hydrogen on Surfaces of Cosmic Dust" and "QCM-2013-3-0015: Adsorption of Atomic Hydrogen on Defective Non-Stoichiometric Surfaces of Cosmic Dust" projects. The use of the Catalonia Supercomputer Centre (CESCA) is gratefully acknowledged.

Table 1. Computed adsorption energies of one H atom on Fo for the different P1, P2 and C1 adducts at the B3LYP-D2*/B1, B3LYP-D2*/B2//B3LYP-D2*/B1 and B3LYP-D2*/B2 levels of theory. B3LYP BSSE uncorrected adsorption energy (ΔE_{el}); contribution of dispersion to the adsorption energy (ΔE_{D2*}); B3LYP-D2* BSSE uncorrected adsorption energy ($\Delta E = \Delta E_{el} + \Delta E_{D2*}$); BSSE corrected adsorption energy ($\Delta E^C = \Delta E$ + BSSE); BSSE values and percentage (%); zero-point energy corrected adsorption energy ($\Delta U_0 = \Delta E + \Delta$ZPE) and ($\Delta U_0{}^C = \Delta E^C + \Delta$ZPE). Bare values in kcal mol^{-1}, meV in parenthesis and K in brackets.

Adduct	Level	ΔE_{el}	ΔE_{D2*}	ΔE	ΔE^C	BSSE	%	ΔU_0	$\Delta U_0{}^C$
P1	B1	-1.7	-1.6	-3.3	-1.9	1.4	41	-2.2	-0.8
	B2//B1	-1.7	-1.6	-3.3	-2.7	0.6	17	-2.2	-1.6
	B2	-1.8	-1.5	-3.4	-2.7	0.7	19	-2.4	-1.7
					(-117)				(-74)
					[-1359]				[-856]
P2	B1	-3.8	-0.6	-4.3	-3.2	1.1	26	-2.6	-1.5
	B2//B1	-3.7	-0.6	-4.3	-3.8	0.5	10	-2.6	-2.1
	B2	-3.6	-0.5	-4.1	-3.7	0.4	10	-2.3	-1.9
					(-160)				(-82)
					[-1862]				[956]
C1	B1	-15.5	-0.1	-15.6	-12.5	3.1	20	-9.2	-6.1
	B2//B1	-16.6	-0.1	-16.7	-15.4	1.3	8	-10.3	-9.0
	B2	-16.3	-0.3	-16.5	-15.1	1.4	9	-10.4	-9.0
					(-654)				(-390)
					[-7599]				[-4529]

Table 2. BSSE uncorrected adsorption energies (ΔE, in kcal mol^{-1}) with B2 basis set spin densities on the H atom (ρ_H) and on the Mg atom closest to H (ρ_{Mg}), and sum of the spin density values of the O atoms closest to the H atom (ρ_O) for the P1, P2 and C1 adducts optimized at the B3LYP-D2*/B1 level.

Method	Adduct	ΔE	ρ_H	ρ_{Mg}	ρ_O
PBE-D2*	P1	-4.3	0.86	0.10	0.04
	P2	-5.0	0.71	0.09	0.20
	C1	-18.7	0.03	0.91	0.06
BLYP-D2*	P1	-3.0	0.84	0.10	0.06
	P2	-5.0	0.69	0.11	0.20
	C1	-15.8	0.03	0.89	0.08
B3LYP-D2*	P1	-3.3	0.88	0.08	0.04
	P2	-4.3	0.73	0.07	0.20
	C1	-16.7	0.02	0.92	0.06
BHLYP-D2*	P1	-2.5	0.91	0.06	0.03
	P2	-1.9	0.78	0.05	0.17
	C1	-15.2	0.01	0.95	0.04

Table 3. B3LYP-D2* zero point energy corrected energy barriers ($\Delta U_0^{\neq}$, in kcal mol^{-1}, (meV), [K]) at B2//B1 level. Rate constants computed using the classical Eyring equation from the conventional transition state theory (k^{TST}, in s^{-1}). Calculated tunneling transmission coefficient (κ, in s^{-1}) using the Wigner correction. Calculated final rate constant as $k = \kappa \times k^{TST}$ (in s^{-1}).

Reaction	$\Delta U_0^{\neq}$			T = 10 K			T = 100 K		
				k^{TST}	κ	k	k^{TST}	κ	k
Figure 3									
P1 → P2	4.1	(178)	[2063]	5.1×10^{-79}	17.3	8.9×10^{-78}	2.3×10^{3}	1.2	2.7×10^{3}
P2 → C1	6.4	(278)	[3221]	2.8×10^{-129}	968.4	2.7×10^{-126}	2.1×10^{-2}	10.7	2.3×10^{-1}
Fo + H → C1	6.0	(260)	[3019]	1.5×10^{-120}	1540.7	2.4×10^{-117}	1.6×10^{-1}	16.4	2.6
Figure 4									
C1-P2a → C1-P2b	18.3	(793)	[9209]	0	2186	0	2.1×10^{-28}	22.9	4.8×10^{-27}
Figure 5									
P2-P1 → Fo-H_2	0.7	(28)	[327]	1.3×10^{-3}	63.6	8.3×10^{-2}	7.9×10^{10}	1.6	1.3×10^{11}
P2-P2 → Fo-H_2	0.5	(21)	[242]	6.3	113.8	7.1×10^{2}	1.9×10^{11}	2.1	3.9×10^{11}
Figure 6									
C1-P2a → Fo-H_2	22.5	(974)	[11307]	0	814.7	0	1.6×10^{-37}	9.1	1.5×10^{-36}
C1-P2b → Fo-H_2	1.7	(74)	[854]	1.8×10^{-26}	1065.5	1.9×10^{-23}	4.1×10^{8}	11.6	4.8×10^{9}
C1-C1 → Fo-H_2	34.9	(1510)	[17529]	0	34.6	0	1.6×10^{-64}	1.3	2.1×10^{-64}

Table 4. B3LYP-D2* reaction energies calculated at B1 and B2//B1 levels for the adsorption of a second H atom on Fo-H models to form the P1-P1, P2-P1, P2-P2, C1-P2a, C1-P2b and C1-C1 complexes. Uncorrected (ΔE), BSSE corrected (ΔE^C) and zero-point energy corrected ($\Delta U_0{}^C$) adsorption energies. Bare values in kcal mol^{-1}, in parenthesis in meV, in brackets in K.

Reaction	ΔE			ΔE^C			$\Delta U_0{}^C$		
P1 + H → P1-P1									
B1	-3.1	(-134)	[-1560]	-1.8	(-78)	[-906]	-1.1	(-48)	[-554]
B2//B1	-3.4	(-147)	[-1711]	-2.9	(-126)	[-1459]	-2.2	(-95)	[-1107]
P2 + H → P2-P1									
B1	-3.1	(-134)	[-1560]	-1.8	(-78)	[-906]	-1.0	(-43)	[-503]
B2//B1	-3.3	(-143)	[-1661]	-2.8	(-121)	[-1409]	-2.0	(-87)	[-1007]
P2 + H → P2-P2									
B1	-3.9	(-169)	[-1963]	-2.8	(-121)	[-1409]	-1.4	(-61)	[-705]
B2//B1	-3.9	(-169)	[-1963]	-3.6	(-156)	[-1812]	-2.1	(-91)	[-1057]
C1 + H → C1-P2a									
B1	-63.9	(-2766)	[-32159]	-63.0	(-2727)	[-31706]	-59.6	(-2580)	[-29995]
B2//B1	-64.3	(-2784)	[-32360]	-65.2	(-2823)	[-32813]	-61.8	(-2675)	[-31102]
C1 + H → C1-P2b									
B1	-82.3	(-3563)	[-41419]	-81.4	(-3524)	[-40966]	-78.0	(-3377)	[-39255]
B2//B1	-82.4	(-3567)	[-41470]	-82.1	(-3554)	[-41319]	-78.7	(-3407)	[-39607]
C1 + H → C1-C1									
B1	-2.8	(-121)	[-1409]	-0.2	(-9)	[-101]	5.0	(216)	[2516]
B2//B1	-3.9	(-169)	[-1963]	-2.7	(-117)	[-1359]	2.5	(108)	[1258]
Fo + H_2 → Fo-H_2									
B1	-5.6	(-241)	[-2800]	-3.5	(-150)	[-1750]	-1.3	(56)	[650]
B2//B1	-5.0	(-215)	[-2500]	-4.3	(-185)	[-2150]	-2.1	(90)	[1050]

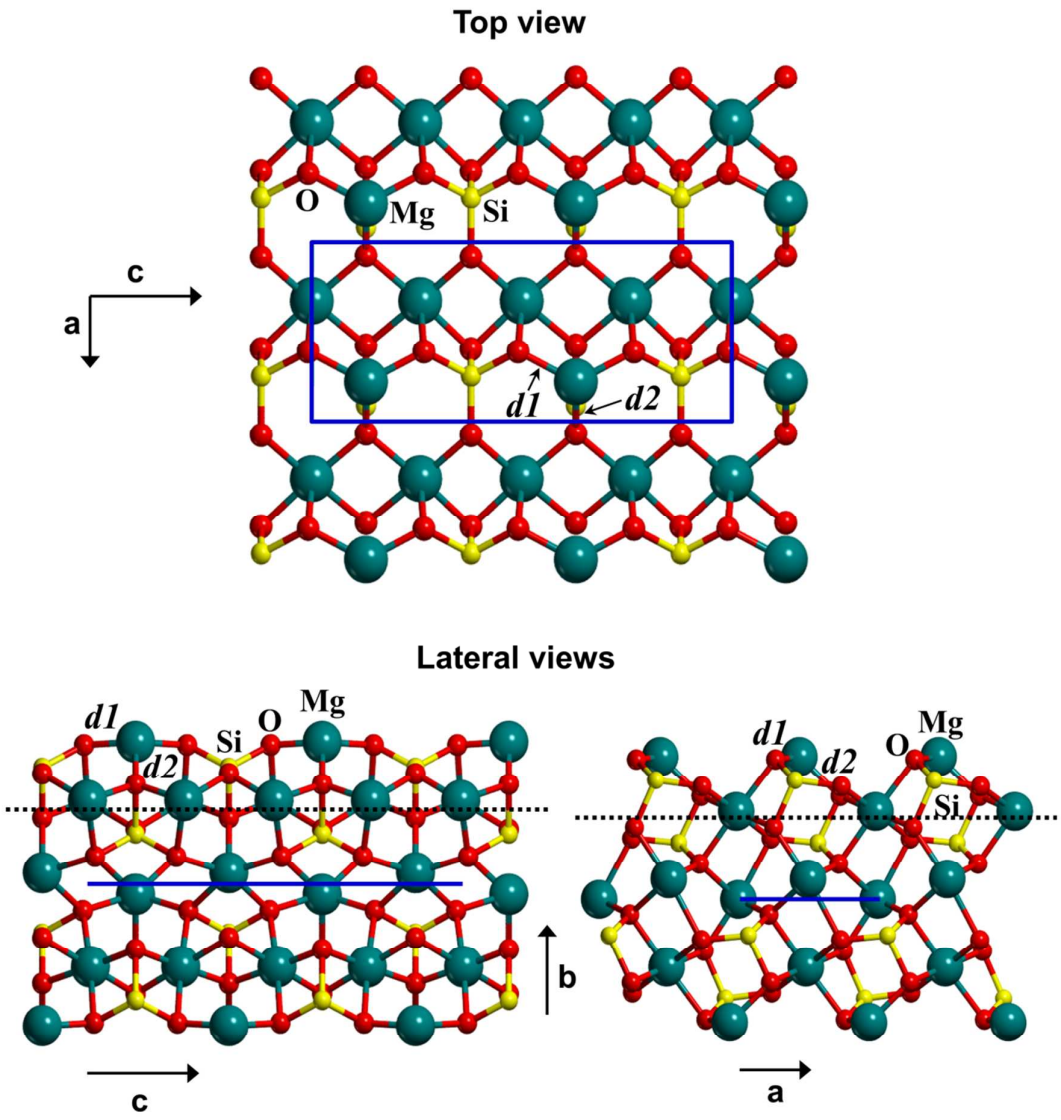

Figure 1. Top and lateral views of the (010) Mg_2SiO_4 surface model used in this work. Unit cell is highlighted in blue. Slab lattice parameters: a = 4.7892 Å and c = 12.0183 Å. The slab thickness was derived from the bulk unit cell b = 10.256 Å axis. B3LYP-D2* optimized Mg-O distances: *d1* = 1.862 Å and *d2* = 1.642 Å. Atoms above the dashed lines are those included in the frequency calculations.

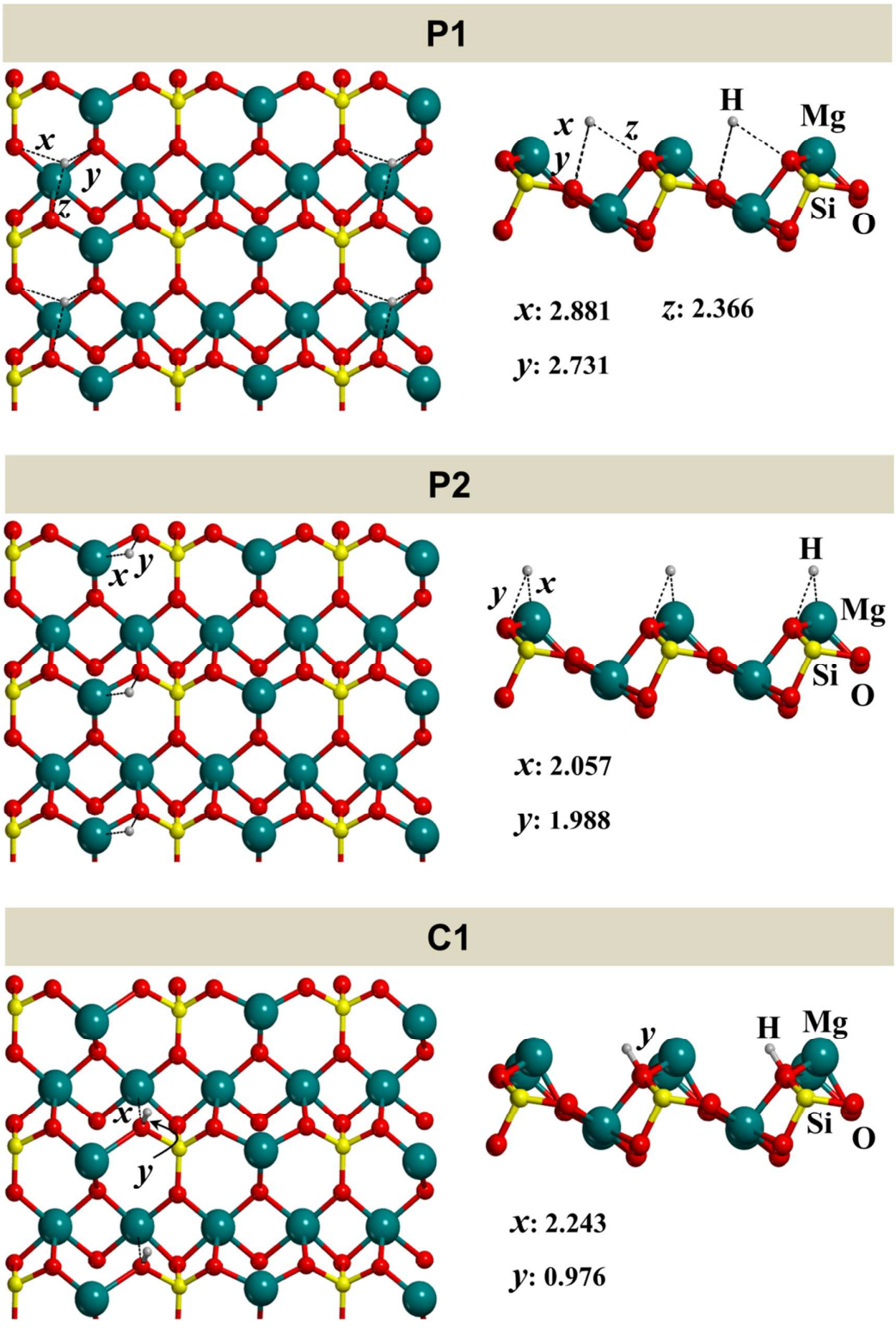

Figure 2. B3LYP-D2* optimized geometries (x, y and z distances in Å) of the different complexes for the H adsorption on the (010) Mg_2SiO_4 surface model (P1, P2 and C1). Left: top view of the adducts. Right: lateral view of a surface fragment.

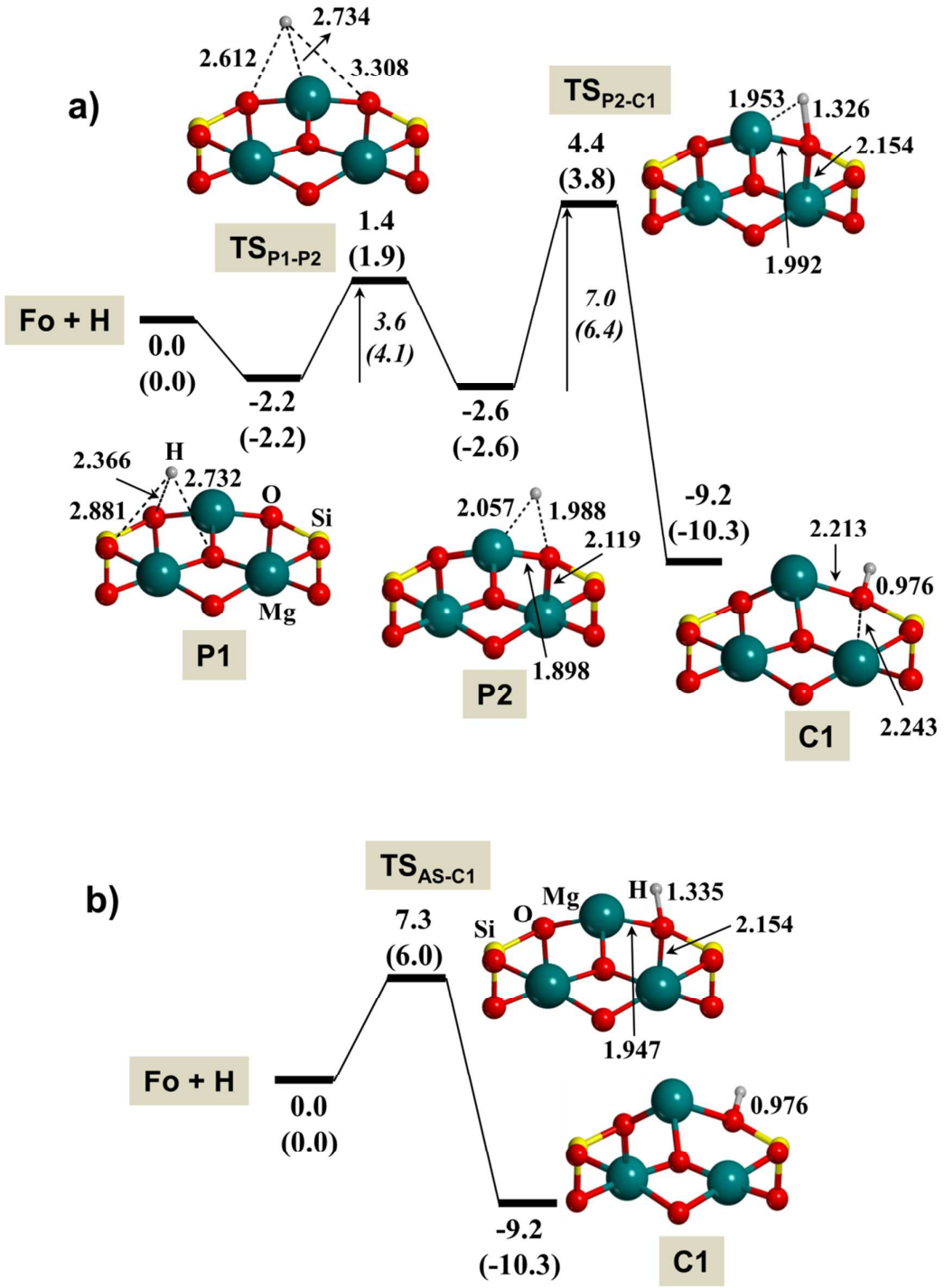

Figure 3. B3LYP-D2* energy profiles including zero-point energy corrections (in kcal mol^{-1}) for: a) the inter-conversion between the different adsorption states adopting a P1 → P2 → C1 sequence; and b) direct H adsorption to form C1. Relative energies are referenced with respect to the Fo + H zero-energy asymptote. Bare values calculated at B1; in parenthesis at B2//B1.

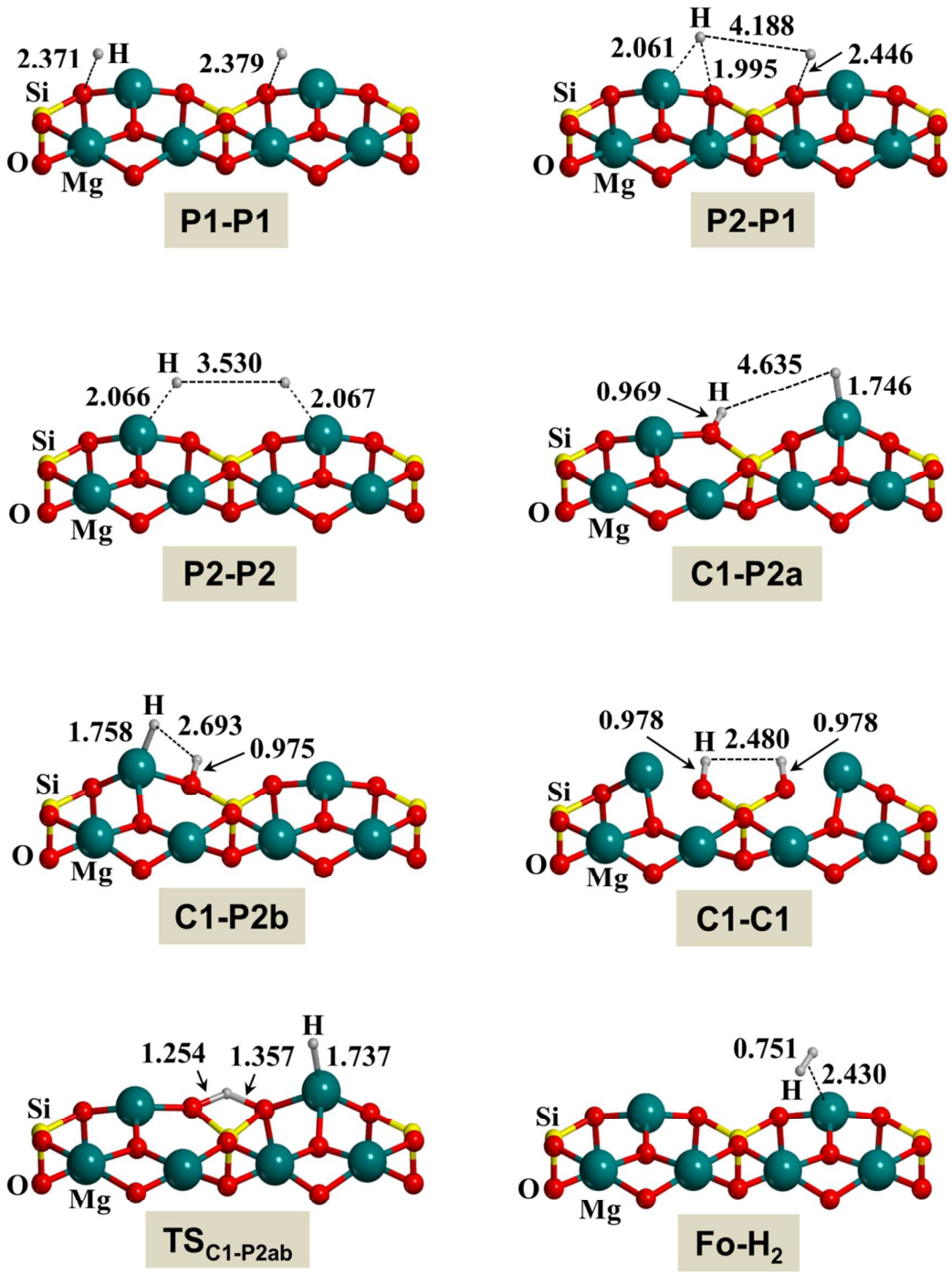

Figure 4. B3LYP-D2* optimized geometries of the different complexes derived from a second H adsorption on the (010) Mg_2SiO_4 surface model (P1-P1, P2-P1, P2-P2, C1-P2a, C1-P2b and C1-C1), for the adsorption of a H_2 molecule (Fo-H_2) and for the transition state converting C1-P2a into C1-P2b ($TS_{C1\text{-}P2ab}$). Bond distances in Å.

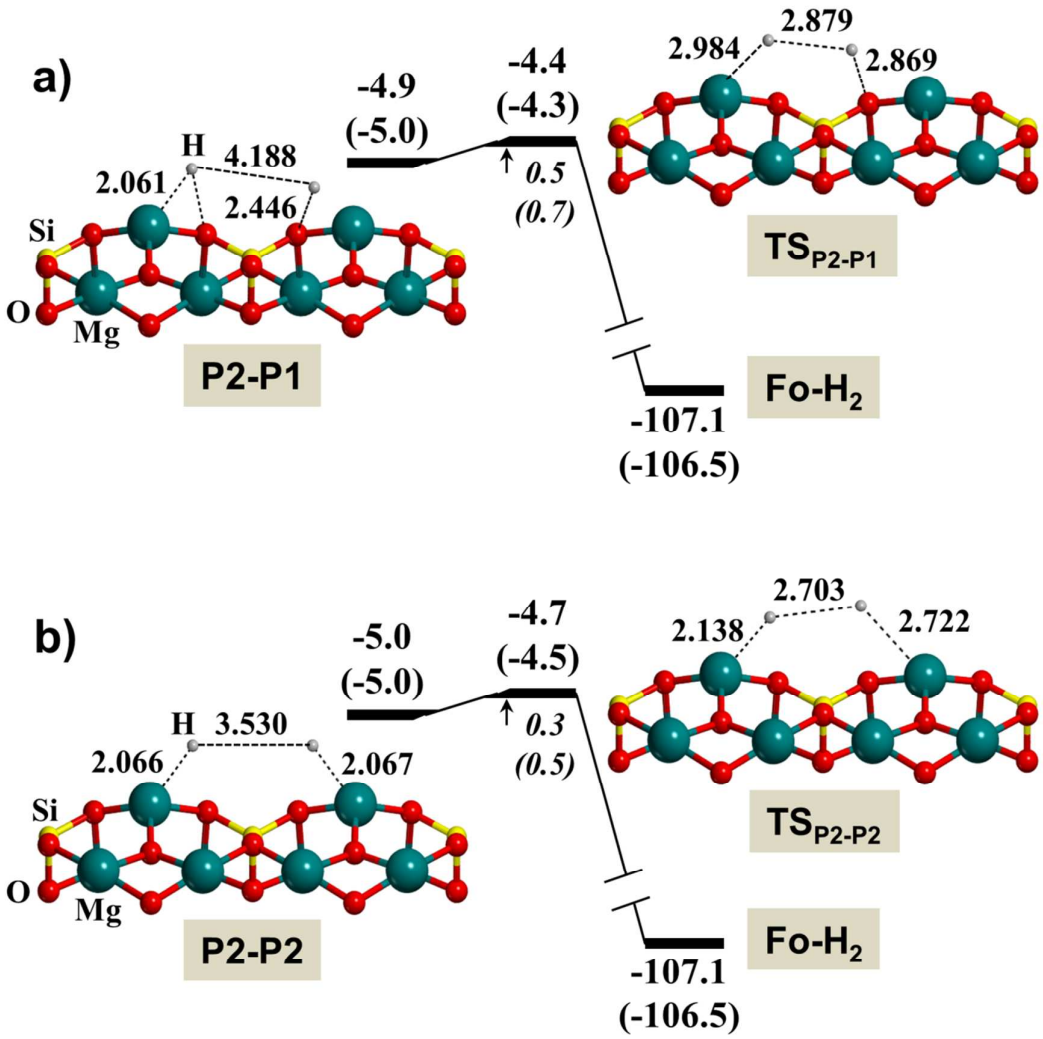

Figure 5. B3LYP-D2* energy profiles including zero-point energy corrections (in kcal mol^{-1}) for the recombination of two physisorbed H atoms to form H_2 on the (010) Mg_2SiO_4 surface model. Relative energies are referenced with respect to the Fo + 2H zero-energy asymptote. Bare values calculated at B1; in parenthesis at B2//B1.

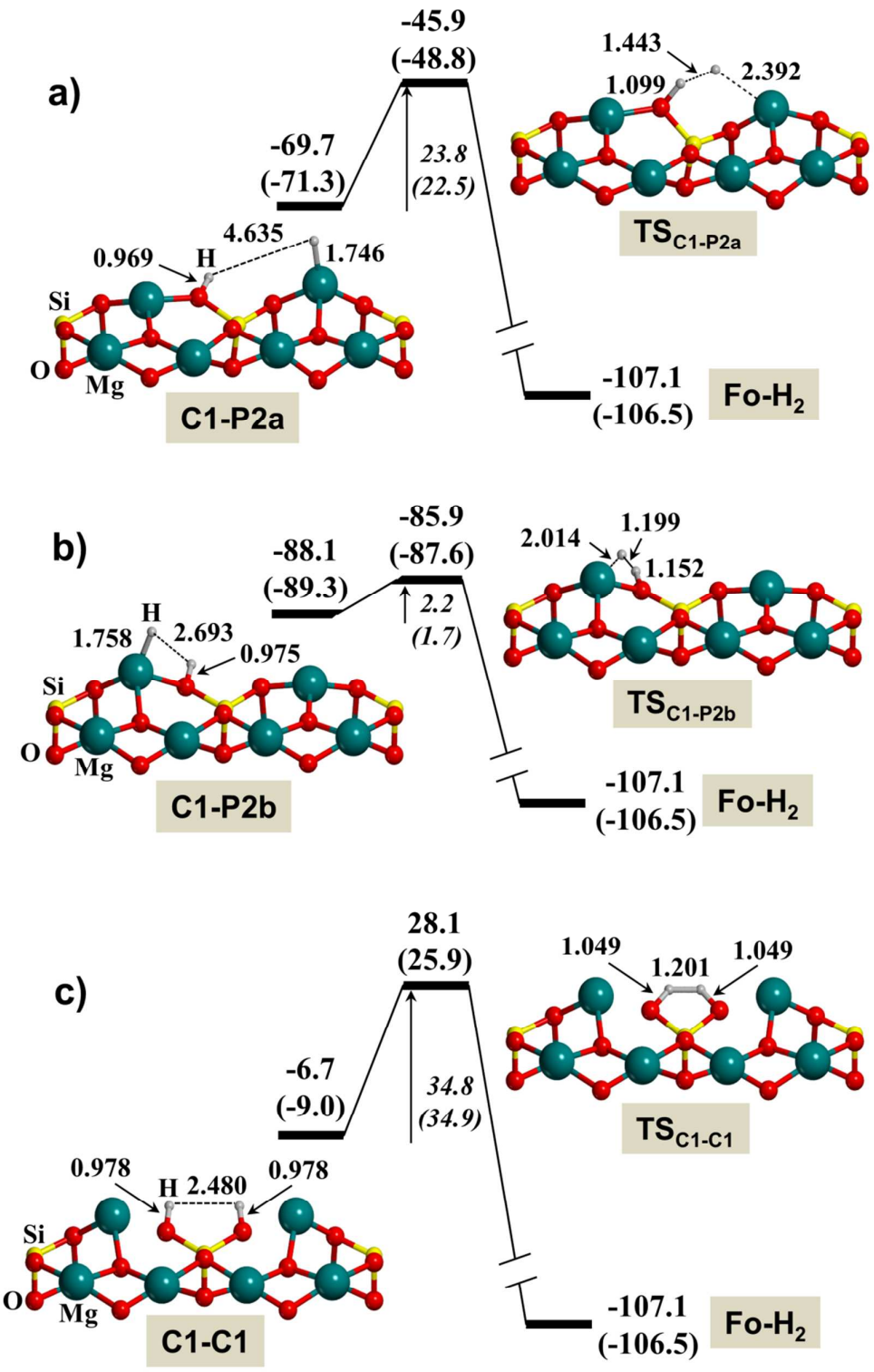

Figure 6. B3LYP-D2* energy profiles including zero-point energy corrections (in kcal mol^{-1}) for the recombination of two H atoms to form H_2 on the (010) Mg_2SiO_4 surface model when at least one H atom is chemisorbed. Relative energies are referenced with respect to the Fo + 2H zero-energy asymptote. Bare values calculated at B1; in parenthesis at B2//B1.

References

1. G. Vidali, J. E. Roser, L. Ling, E. Congiu, G. Manico and V. Pirronello, *Faraday Disc.*, 2006, **133**, 125-135.
2. G. Vidali, *Chem. Rev.*, 2013, **113**, 8762-8782.
3. D. Hollenbach and E. E. Salpeter, *J. Chem. Phys.*, 1970, **53**, 79-86.
4. T. Henning, ed., *Astromineralogy*, Springer-Verlag, Berlin, 2010.
5. T. Henning, *Annu. Rev. Astron. Astrophys.*, 2010, **48**, 21-46.
6. F. Molster and C. Kemper, *Space Science Reviews*, 2005, **119**, 3-28.
7. I. Langmuir, *Transactions of the Faraday Society*, 1922, **17**, 621-654.
8. C. N. Hinshelwood, *Annu. Res. London Chem. Soc.* , 1930, **27**, 11
9. D. D. Eley and E. K. Rideal., *Nature* 1940, **146**, 401-402.
10. D. D. Eley, *Proc. R. Soc. London*, 1941, **178**, 452
11. J. Harris and B. Kasemo, *Surf. Sci.*, 1981, **105**, L281-L287.
12. D. Bachellerie, M. Sizun, F. Aguillon, D. Teillet-Billy, N. Rougeau and V. Sidis, *Phys. Chem. Chem. Phys.*, 2009, **11**, 2715-2729.
13. A. J. H. M. Meijer, A. J. Farebrother, D. C. Clary and A. J. Fisher, *J. Phys. Chem. A*, 2001, **105**, 2173-2182.
14. S. Morisset, F. Aguillon, M. Sizun and V. Sidis, *Phys. Chem. Chem. Phys.*, 2003, **5**, 506-513.
15. S. Morisset, F. Aguillon, M. Sizun and V. Sidis, *J. Chem. Phys.*, 2005, **122**, 194702-194708.
16. S. Casolo, G. F. Tantardini and R. Martinazzo, *Proc. Natl. Acad. Sci. USA*, 2013, **110**, 6674-6677.
17. B. Kerkeni and S. T. Bromley, *Mon. Not. R. Astron. Soc.*, 2013, **435**, 1486-1492.
18. T. P. M. Goumans and S. T. Bromley, *Mon. Not. R. Astron. Soc.*, 2011, **414**, 1285-1291.
19. S. Garcia-Gil, D. Teillet-Billy, N. Rougeau and V. Sidis, *J. Phys. Chem. C*, 2013, **117**, 12612-12621.
20. C. A. Downing, B. Ahmady, C. R. A. Catlow and N. H. de Leeuw, *Phil. Trans. R. Soc. A*, 2013, **371**.
21. T. P. M. Goumans, C. Richard, A. Catlow and W. A. Brown, *Mon. Not. R. Astron. Soc.*, 2009, **393**, 1403-1407.
22. Y. Zhao and D. G. Truhlar, *J. Chem. Theory Comput.*, 2005, **1**, 415-432.
23. A. D. Boese and J. Sauer, *Phys. Chem. Chem. Phys.*, 2013, **15**, 16481-16493.
24. P. Ugliengo and A. Damin, *Chem. Phys. Lett.*, 2002, **366**, 683-690.

25. B. Civalleri, L. Maschio, P. Ugliengo and C. M. Zicovich-Wilson, *Phys. Chem. Chem. Phys.*, 2010, **12**, 6382-6386.
26. S. Grimme, *J. Comput. Chem.*, 2006, **27**, 1787-1799.
27. B. Civalleri, C. M. Zicovich-Wilson, L. Valenzano and P. Ugliengo, *CrystEngComm*, 2008, **10**, 405-410.
28. J. Navarro-Ruiz, P. Ugliengo, A. Rimola and M. Sodupe, *J. Phys. Chem. A*, 2014, DOI: 10.1021/jp4118198.
29. R. Dovesi, V. R. Saunders, C. Roetti, R. Orlando, C. M. Zicovich-Wilson, F. Pascale, B. Civalleri, K. Doll, N. M. Harrison, I. J. Bush, P. D'Arco and M. Llunell, *CRYSTAL09 User's Manual.*, University of Torino, Torino, 2009.
30. R. Dovesi, R. Orlando, B. Civalleri, C. Roetti, V. R. Saunders and C. M. Zicovich-Wilson, *Z. Kristallogr.*, 2005, **220**, 571-573.
31. A. D. Becke, *J. Chem. Phys.*, 1993, **98**, 5648-5652.
32. J. P. Perdew, K. Burke and M. Ernzerhof, *Phys. Rev. Lett.*, 1996, **77** 3865-3868.
33. A. D. Becke, *Phys. Rev. A*, 1988, **38** 3098-3100.
34. C. Lee, W. Yang and R. G. Parr, *Phys. Rev. B*, 1988, **37** 785-789.
35. A. D. Becke, *J. Chem. Phys.*, 1993, **98**, 1372-1377.
36. A. Rimola, C. M. Zicovich-Wilson, R. Dovesi and P. Ugliengo, *J. Chem. Theory Comput.*, 2010, **6**, 1341-1350.
37. A. Schafer, H. Horn and R. Ahlrichs, *J. Chem. Phys.*, 1992, **97**, 2571-2577.
38. K. Doll, *Comput. Phys. Comm.*, 2001, **137**, 74-78.
39. B. Civalleri, P. D'Arco, R. Orlando, V. R. Saunders and R. Dovesi, *Chem. Phys. Lett.*, 2001, **348**, 131-138.
40. M. Corno, C. Busco, V. Bolis, S. Tosoni and P. Ugliengo, *Langmuir*, 2009, **25**, 2188-2198.
41. E. Wigner, *Z. Physik. Chem. (Leipzig)*, 1932, **Bl9**, 203
42. F. Pascale, C. M. Zicovich-Wilson, F. L. Gejo, B. Civalleri, R. Orlando and R. Dovesi, *J. Comput. Chem.*, 2004, **25**, 888-897.
43. N. Katz, I. Furman, O. Biham, V. Pirronello and G. Vidali, *ApJ*, 1999, **522**, 305-312.